

# Angular Momentum Projected Configuration Interaction with Realistic Hamiltonians

Zao-Chun Gao<sup>1,2\*</sup> and Mihai Horoi<sup>1</sup>

<sup>1</sup>*Department of Physics, Central Michigan University, Mount Pleasant, Michigan 48859, USA*

<sup>2</sup>*China Institute of Atomic Energy P.O. Box 275-18, Beijing 102413, China*

(Dated: September 16, 2021)

The Projected Configuration Interaction (PCI) method starts from a collection of mean-field wave functions, and builds up correlated wave functions of good symmetry. It relies on the Generator Coordinator Method (GCM) techniques, but it improves the past approaches by a very efficient method of selecting the basis states. We use the same realistic Hamiltonians and model spaces as the Configuration Interaction (CI) method, and compare the results with the full CI calculations in the *sd* and *pf* shell. Examples of <sup>24</sup>Mg, <sup>28</sup>Si, <sup>48</sup>Cr, <sup>52</sup>Fe and <sup>56</sup>Ni are discussed.

PACS numbers: 21.60.Cs, 21.60.Ev, 21.10.-k

## I. INTRODUCTION

The full configuration interaction (CI) method using a spherical single particle (s.p.) basis and realistic Hamiltonians has been very successful in describing various properties of the low-lying states in light and medium nuclei. The realistic Hamiltonians, such as the USD [1, 2] in the *sd* shell, the KB3 [3], FPD6 [4] and GXPF1 [5] in the *pf* shell, have provided a very good base to study various nuclear structure problems microscopically.

Some *sd* and *pf* nuclei such as <sup>28</sup>Si and <sup>48</sup>Cr are well deformed. Their collective behavior is confirmed by the strong collective E2 transitions and the rotational behavior of the yrast state energies,  $E(I) \sim I(I+1)$ . The mean-field description in the intrinsic frame naturally takes advantage of the spontaneous symmetry breaking. This approach provides some physical insight, but the loss of good angular momentum of the mean-field wave functions makes the comparison with the experimental data difficult. The CI calculations in spherical basis provide the description in the laboratory frame. The angular momentum is conserved, but the physical insight associated with the existence of an intrinsic state is lost.

There is a long-lasting effort to connect the mean-field and CI techniques. Elliott was the first to point out the advantage of a deformed intrinsic many body basis and developed the SU(3) Shell Model [6] for *sd* nuclei. In Elliott's model, the rotational motion was associated with strict SU(3) symmetry, approximately realized only near <sup>20</sup>Ne and <sup>24</sup>Mg. This model was limited only to the *sd* shell.

The Projected Shell Model (PSM) [7] can be considered as a natural extension of the SU(3) shell model to heavier systems. In this model, the quadrupole force, that Elliott's model used, the monopole pairing and the quadrupole pairing forces were included in the PSM Hamiltonian. The deformed intrinsic Nilsson+BCS basis are projected onto good angular momentum, and the PSM Hamiltonian is diagonalized in the space spanned

by the projected states. The Nilsson model [8] has been proven to be very successful in describing the deformed intrinsic single particle states, and the quadrupole force was found to be essential for describing the rotational motion [6]. Despite its simplicity PSM was proven to be a very efficient method in analyzing the phenomena associated with the rotational states, especially the high spin states, not only for axial quadrupole deformation, but also for the octupole [9] and triaxial shapes [10, 11]. However, its predictive power is limited because the multipole-multipole plus pairing Hamiltonian has to be tuned to a specific class of states, rather than a region of the nuclear chart.

Besides the Projected Shell Model, another sophisticated approach based on the projection method is MONSTER and the family of VAMPIRs [12]. The MONSTER is similar to the PSM, but the basis is obtained by projecting the Hartree-Fock-Bogoliubov (HFB) vacuum and the related 2-quasiparticle configurations onto good quantum numbers, including neutron and proton number, parity, and the angular momentum. VAMPIR, which performs the energy variation after the projection, is more sophisticated than MONSTER. However, the particle number plus angular momentum projection implemented in MONSTER and VAMPIR requires at least 3-dimensional integration in the axial symmetric case. This makes it very difficult to extend these models to non-axial cases, where the projection with 5-dimensional integration would be needed. MONSTER and VAMPIR can use realistic Hamiltonians.

Instead of using quasiparticle configurations, as PSM and MONSTER/VAMPIR do, the Quantum Monte Carlo Diagonalization (QMCD) method [13] takes the advantage of the Hartree-Fock (HF) mean-field that breaks the symmetries of Hamiltonian. The mean-field is not restricted to axial symmetry. QMCD starts from an appropriate initial state, as in the shell-model Monte Carlo approach [14], to select an optimal set of basis states, and the full Hamiltonian is diagonalized in this basis. More basis states are iteratively added until convergence is achieved. It is very interesting that only the *M*-projection is applied to in the basis states, yet the total angular momentum seems to be fully recovered from the

---

\*Electronic address: gao1z@cmich.edu

diagonalization when the convergence limit is achieved. However, the process of selecting the basis states is reportedly very time consuming.

The Generator Coordinate Method (GCM)[15] is a standard method to describe collective states that goes beyond the mean-field. The angular momentum projection technique is a special case of GCM when the generator coordinates include the Euler angles. In the standard GCM, the excited states are constructed in a basis of HFB vacua, which differ in one or several collective coordinates. However, in many cases, it has been found that the excitation energies provide by GCM are too high. The GCM wave functions may be more appropriate to describe more correlations in the ground state, rather than the excited states. However, our investigations (see below) show that neither the g.s. nor the excited states are accurately described by this simple GCM procedure when realistic effective Hamiltonians and HF vacua are used.

In the present work, we developed a new method called the Projected Configuration Interaction (PCI), which uses GCM and PSM techniques. The PCI basis includes angular momentum projected states generated from a class of constraint HF vacua. However, in addition to these GCM-like states PCI includes a large number of low-lying  $np - nh$  excitations built on those states. In PCI the deformed intrinsic states are Slater Determinants (SD), and the particle number projection is no longer required. This method can use the same realistic Hamiltonian as any CI method. This feature makes the direct comparison between CI and PCI possible. One advantage of this method is that it keeps the number of basis states small, even for cases when the CI dimensions are too large for the today's computers.

The paper is organized as follow. Section II presents the formalism used by PCI. The efficiency of the angular momentum projection is discussed in section III. Section IV analyzes the choice of the PCI basis and presents some results for the *sd* and *pf* nuclei. Section V is devoted to the analysis of the quadrupole moments and E2 transitions. Conclusions and outlook are given in section VI.

## II. THE METHOD OF THE PROJECTED CONFIGURATION INTERACTION (PCI)

The model Hamiltonian used in CI calculations can be written as:

$$H = \sum_i e_i c_i^\dagger c_i + \sum_{i>j,k>l} V_{ijkl} c_i^\dagger c_j^\dagger c_l c_k, \quad (1)$$

where,  $c_i^\dagger$  and  $c_i$  are creation and annihilation operators of the spherical harmonic oscillator,  $e_i$  and  $V_{ijkl}$  are one-body and two-body matrix elements that can be obtained from effective interaction theory, such as G-Matrix plus core polarization [16]; it can be further refined using the experimental data [5, 17].

One can introduce the deformed single particle (s.p.) basis, which can be obtained from a constraint HF solution. Alternatively, one can take the single particle states obtained from the following s.p. Hamiltonian,

$$H_{\text{s.p.}} = h_{\text{sph}} - \frac{2}{3}\epsilon_2 \hbar\omega_0 \sqrt{\frac{4\pi}{5}} \rho^2 Y_{20}(\theta) + \epsilon_4 \hbar\omega_0 \sqrt{\frac{4\pi}{9}} \rho^2 Y_{40}(\theta). \quad (2)$$

Here

$$h_{\text{sph}} = \sum_i E_i c_i^\dagger c_i, \quad (3)$$

is the spherical single particle part of the Hamiltonian with the same eigenfunctions as the spherical harmonic oscillator, but the energy of each orbit is chosen such that the result from this Hamiltonian is near to the HF solution;  $\epsilon_2$  and  $\epsilon_4$  are the quadrupole and hexadecupole deformation parameters,  $\rho = \sqrt{\frac{m\omega_0}{\hbar}} r$  is dimensionless, and we take [18, 19]

$$\hbar\omega_0 = 45A^{1/3} - 25A^{2/3}. \quad (4)$$

The deformed s.p. creation operator is given by the following transformation:

$$b_k^\dagger = \sum_i W_{ki} c_i^\dagger, \quad (5)$$

where the matrix elements  $W_{ki} = \langle b_k | c_i \rangle$  are real in our calculation. Inserting the reversed transformation of Eq. (5)

$$c_i^\dagger = \sum_k W_{ik}^t b_k^\dagger \quad (6)$$

into the model Hamiltonian Eq. (1), we obtain the transformed  $H$  in the deformed s.p. basis

$$H = \sum_{ij} h_{ij}^{(1)} b_i^\dagger b_j + \sum_{i>j,k>l} h_{ijkl}^{(2)} b_i^\dagger b_j^\dagger b_l b_k. \quad (7)$$

Here  $h^{(1)}$  and  $h^{(2)}$  are one-body and two-body matrix elements of  $H$  in the deformed basis. The Slater Determinant (SD) built on the deformed single particle states is given by

$$|\kappa\rangle \equiv |s, \epsilon\rangle \equiv b_{i_1}^\dagger b_{i_2}^\dagger \dots b_{i_n}^\dagger | \rangle, \quad (8)$$

where  $s$  refers to the Nilsson configuration, indicating the pattern of the occupied orbits, and  $\epsilon$  is the deformation determined by  $\epsilon_2$  and  $\epsilon_4$ . The matrix element  $\langle \kappa | H | \kappa' \rangle$ , can be calculated using Eq.(7).

Generally,  $|\kappa\rangle$  doesn't have good angular momentum  $I$ . It is well known that the projection on good angular momentum would add correlations to the wave function.

The general form of the nuclear wave function is therefore a linear combination of the projected SDs (PSDs),

$$|\Psi_{IM}^\sigma\rangle = \sum_{K\kappa} f_{IK\kappa}^\sigma P_{MK}^I |\kappa\rangle, \quad (9)$$

where

$$\hat{P}_{MK}^I = \frac{2I+1}{8\pi^2} \int d\Omega D_{MK}^I(\Omega) \hat{R}(\Omega) \quad (10)$$

is the angular momentum projection operator.  $D_{MK}^I$  is the D-function, defined as

$$D_{MK}^I(\Omega) = \langle IM | \hat{R}(\Omega) | IK \rangle^*, \quad (11)$$

$\hat{R}$  is the rotation operator, and  $\Omega$  is the solid angle. If one keeps the axial symmetry in the deformed basis,  $D_{MK}^I$  in Eq(10) reduces to  $d_{MK}^I(\beta) = \langle IM | e^{-i\beta \hat{J}_y} | IK \rangle$  and the three dimensional  $\Omega$  reduces to  $\beta$ .

The energies and the wave functions [given in terms of the coefficients  $f_{IK\kappa}^\sigma$  in Eq.(9)] are obtained by solving the following eigenvalue equation:

$$\sum_{K'\kappa'} (H_{K\kappa, K'\kappa'}^I - E_I^\sigma N_{K\kappa, K'\kappa'}^I) f_{IK\kappa'}^\sigma = 0, \quad (12)$$

where  $H_{K\kappa, K'\kappa'}^I$  and  $N_{K\kappa, K'\kappa'}^I$  are the matrix elements of the Hamiltonian and of the norm, respectively

$$H_{K\kappa, K'\kappa'}^I = \langle \kappa | H P_{KK'}^I | \kappa' \rangle, \quad (13)$$

$$N_{K\kappa, K'\kappa'}^I = \langle \kappa | P_{KK'}^I | \kappa' \rangle. \quad (14)$$

The matrix element of  $H_{K\kappa, K'\kappa'}^I$  and  $N_{K\kappa, K'\kappa'}^I$  can be expanded as

$$\begin{aligned} & \langle \kappa | H P_{KK'}^I | \kappa' \rangle \\ &= \frac{2I+1}{8\pi^2} \int d\Omega D_{KK'}^I(\Omega) \langle \kappa | H \hat{R}(\Omega) | \kappa' \rangle, \end{aligned} \quad (15)$$

$$\begin{aligned} & \langle \kappa | P_{KK'}^I | \kappa' \rangle \\ &= \frac{2I+1}{8\pi^2} \int d\Omega D_{KK'}^I(\Omega) \langle \kappa | \hat{R}(\Omega) | \kappa' \rangle, \end{aligned} \quad (16)$$

where

$$\langle \kappa | H \hat{R}(\Omega) | \kappa' \rangle = \sum_{\kappa''} \langle \kappa | H | \kappa'' \rangle \langle \kappa'' | \hat{R}(\Omega) | \kappa' \rangle. \quad (17)$$

Here  $\kappa''$  has the same deformation as  $\kappa$ , and runs over all SDs with nonzero  $\langle \kappa | H | \kappa'' \rangle$ . Therefore, the main problem is to calculate the matrix element of the rotation  $\hat{R}(\Omega)$  between different SDs,  $\langle \kappa | \hat{R}(\Omega) | \kappa' \rangle$ .

$|\kappa\rangle$  and  $|\kappa'\rangle$  may have different shapes. We denote  $a^\dagger, a$  the single particle operators with deformation  $\epsilon_a$  that create the SD  $|\kappa\rangle$ , and  $b^\dagger, b$ , with deformation  $\epsilon_b$ , that create  $|\kappa'\rangle$ . Expressing  $\langle \kappa | \hat{R}(\Omega) | \kappa' \rangle$  with  $a^\dagger, a$  and

$b^\dagger, b$ , one gets

$$\begin{aligned} & \langle \kappa | \hat{R}(\Omega) | \kappa' \rangle \\ &= \langle | a_{i_n} \dots a_{i_2} a_{i_1} \hat{R}(\Omega) b_{j_1}^\dagger b_{j_2}^\dagger \dots b_{j_n}^\dagger | \rangle \\ &= \langle | a_{i_n} \dots a_{i_2} a_{i_1} \\ & \quad \hat{R}(\Omega) b_{j_1}^\dagger \hat{R}^{-1}(\Omega) \hat{R}(\Omega) b_{j_2}^\dagger \hat{R}^{-1}(\Omega) \dots \hat{R}(\Omega) b_{j_n}^\dagger \hat{R}^{-1}(\Omega) | \rangle \\ &= \langle | a_{i_n} \dots a_{i_2} a_{i_1} \\ & \quad \left( \sum_{k_1} R_{k_1 j_1} a_{k_1}^\dagger \right) \left( \sum_{k_2} R_{k_2 j_2} a_{k_2}^\dagger \right) \dots \left( \sum_{k_n} R_{k_n j_n} a_{k_n}^\dagger \right) | \rangle \\ &= \begin{vmatrix} R_{i_1 j_1} & R_{i_1 j_2} & \dots & R_{i_1 j_n} \\ R_{i_2 j_1} & R_{i_2 j_2} & \dots & R_{i_2 j_n} \\ \dots & \dots & \dots & \dots \\ R_{i_n j_1} & R_{i_n j_2} & \dots & R_{i_n j_n} \end{vmatrix}. \end{aligned} \quad (18)$$

Here

$$\begin{aligned} & \hat{R}(\Omega) b_j^\dagger \hat{R}^{-1}(\Omega) \\ &= \sum_l W_{jl}^b \hat{R}(\Omega) c_l^\dagger \hat{R}^{-1}(\Omega) \\ &= \sum_{lk} W_{jl}^b D_{kl}^*(\Omega) c_k^\dagger \\ &= \sum_i \left( \sum_{lk} W_{jl}^b D_{kl}^*(\Omega) W_{ik}^a \right) a_i^\dagger \\ &= \sum_i R_{ij} a_i^\dagger. \end{aligned} \quad (19)$$

Note that the rotation never mixes the neutron and proton wave functions. Therefore, the matrix elements in Eq.(18) can be calculated for neutron and proton separately.

The choice of the PCI basis will be described in Section IV.

### III. THE EFFICIENCY OF THE PROJECTION ON GOOD ANGULAR MOMENTUM

Let's analyze the quality of the deformed single particle states for the USD Hamiltonian [2]. The  $E_i$  energies (see Eq.(3)) are properly adjusted so that the SD with the lowest energy is close to the HF vacuum, as will be discussed in this Section. For  $sd$  shell, we use  $E_{d_{5/2}} = -3.9$  MeV,  $E_{s_{1/2}} = -1.2$  MeV and  $E_{d_{3/2}} = 1.6$  MeV, and the corresponding Nilsson levels as functions of quadrupole deformation  $\epsilon_2$  ( $\epsilon_4 = 0$ ) are plotted in Fig.1.

To find the lowest value  $E_{\text{def}}$  of  $\langle \kappa | H | \kappa \rangle$ , the energy surface of

$$E_{\text{exp}}(s, \epsilon) = \langle s, \epsilon | H | s, \epsilon \rangle \quad (20)$$

needs to be calculated for each configuration  $s$ . Here, we use the USD Hamiltonian, and take  $^{28}\text{Si}$  as a case study. The SD with all 12 particles occupying the Nilsson orbits originating from the  $d_{5/2}$  spherical

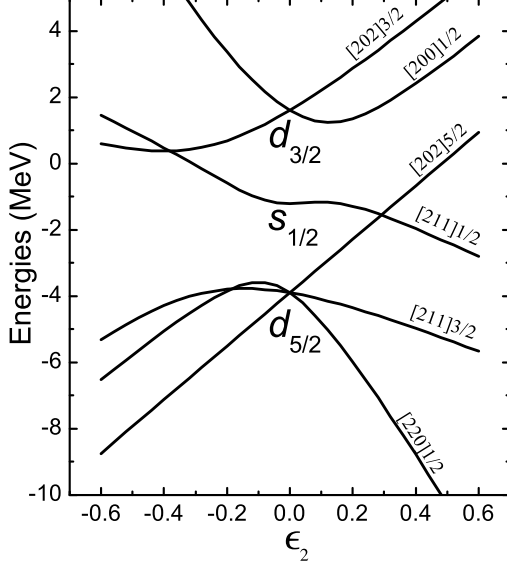


FIG. 1: The Nilsson levels for  $sd$  shell

orbit are used in Eq. (20). Such an SD is denoted by  $s_0$  hereafter. This configuration provides the lowest energy for a large range of deformations and is expected to describe very well the mean-field minimum, i.e. the ground state (g.s.),  $\langle \kappa | H | \kappa \rangle$  at certain deformation(s). The energy surface of the  $s_0$  configuration as a function of  $(\epsilon_2, \epsilon_4)$  is shown as the upper surface in Fig. 2. The minimum energy,  $E_{\text{def}} = -129.55$  MeV at deformation  $(\epsilon_2, \epsilon_4)_{\text{def}} = (-0.44, -0.10)$ , which is very close to the HF energy ( $E_{\text{HF}} = -129.61$  MeV) [18]. Besides, the calculated quadrupole moment,  $-70.1 \text{ fm}^2$ , is also very close to the HF value,  $-69.6 \text{ fm}^2$  [18]. Thus, we reached an approximated solution to the HF mean-field from a simple Nilsson Hamiltonian. For other deformed  $sd$  nuclei the situation is similar to  $^{28}\text{Si}$ , as shown in Table I.

The ground state of  $^{28}\text{Si}$  should have good angular momentum with spin  $I = 0$ . We calculate the expectation value of  $H$  with respect to the projected SD:

$$E_{\text{exp}}(I, s, \epsilon) = \frac{\langle s, \epsilon | H P_{KK}^I | s, \epsilon \rangle}{\langle s, \epsilon | P_{KK}^I | s, \epsilon \rangle}, \quad (21)$$

where  $K$  is defined by  $\hat{J}_z |s, \epsilon\rangle = K |s, \epsilon\rangle$ . The energy surface of  $E_{\text{exp}}(I = 0, s_0, \epsilon)$  is shown as the lower surface in Fig. 2. The minimum value  $E_{\text{pj}}(I = 0) = -133.64$  MeV at  $(\epsilon_2, \epsilon_4)_{\text{pj}} = (-0.40, -0.20)$ , which is about 4 MeV lower than the HF energy, and 2.30 MeV above the exact ground state energy of the USD Hamiltonian at  $-135.94$  MeV. Similar calculations for other deformed  $sd$ -shell nuclei are reported in Table. I. These results indicate that the restoration of the angular momentum has a significant contribution to the ground state (g.s.) correlation energy.

An even stronger argument in favor of imposing good

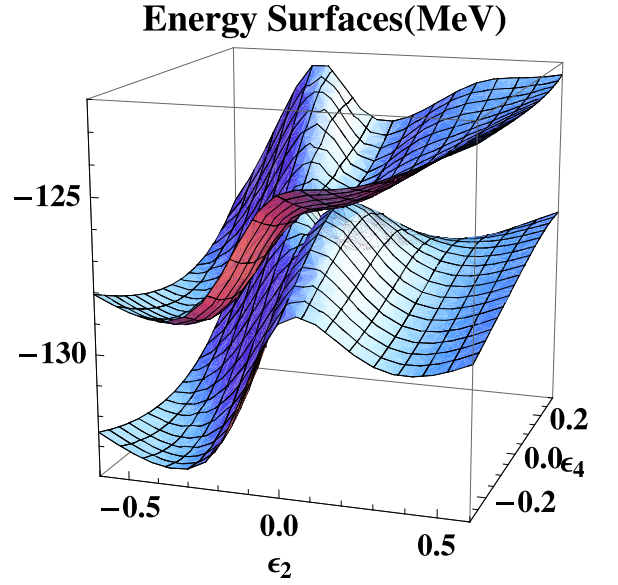


FIG. 2: (Color online) Energy surfaces of the USD Hamiltonian with respect to the unprojected  $SD(s_0)$  (upper surface) and the projected  $SD(s_0)$  with  $I=0$  (lower surface), as functions of quadrupole  $\epsilon_2$  and hexadecupole  $\epsilon_4$  deformation.

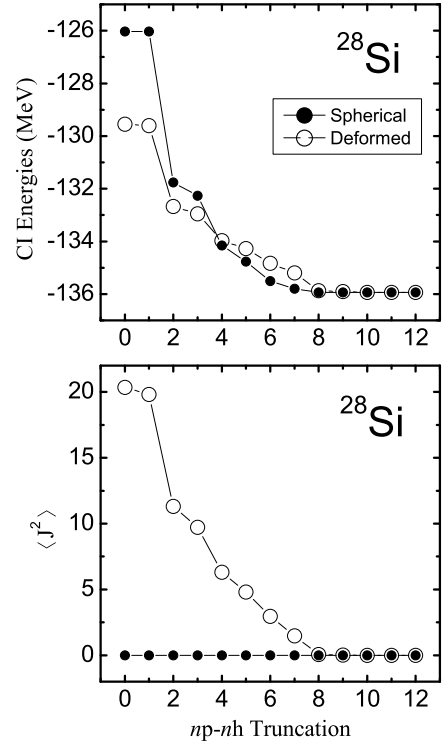


FIG. 3: The ground state energies (upper panel) and the corresponding  $\langle J^2 \rangle$  values (lower panel) of  $^{28}\text{Si}$  from spherical and deformed CI as functions of different  $np$ - $nh$  truncation

TABLE I: Energies (in MeV) with USD Hamiltonian for some deformed *sd* Nuclei.  $E_{\text{sph}}$  is the spherical HF energy,  $E_{\text{HF}}$  is the minimum of the deformed HF energy,  $E_{\text{def}}$  is the lowest energy of Eq.(20) and  $(\epsilon_2, \epsilon_4)_{\text{def}}$  is the deformation for  $E_{\text{def}}$ ,  $E_{\text{pj}}(I=0)$  is the lowest energy of Eq.(21) at spin  $I=0$  and  $(\epsilon_2, \epsilon_4)_{\text{pj}}$  is the deformation for  $E_{\text{pj}}(I=0)$ .  $E_{\text{Full CI}}$  is the exact solution of the USD Hamiltonian.

Nucleus	$E_{\text{sph}}^a$	$E_{\text{HF}}^a$	$E_{\text{def}}$	$(\epsilon_2, \epsilon_4)_{\text{def}}$	$E_{\text{pj}}(I=0)$	$(\epsilon_2, \epsilon_4)_{\text{pj}}$	$E_{\text{Full CI}}$
$^{20}\text{Ne}$	-31.79 <sup>b</sup>	-36.38	-36.38	(0.60, -0.04)	-39.86	(0.56, -0.26)	-40.49
$^{24}\text{Mg}$	-68.20	-80.17	-79.80	(0.50, 0.08)	-83.04	(0.58, 0.04)	-87.09
$^{28}\text{Si}$	-126.03	-129.61	-129.55	(-0.44, -0.10)	-133.64	(-0.40, -0.20)	-135.94
$^{36}\text{Ar}$	-222.75	-226.56	-226.56	(-0.32, 0.08)	-229.78	(-0.20, 0.30)	-230.51

<sup>a</sup>Data taken from Ref.[18].

<sup>b</sup>The -25.46 MeV in Ref. [18] has been corrected as -31.79 MeV.

angular momentum to the wave functions can be found by comparing the results of CI calculations using spherical and deformed s.p. bases, as shown in Fig. 3. The deformation for the deformed CI basis is  $(\epsilon_2, \epsilon_4)_{\text{def}} = (-0.44, -0.10)$  as shown in Table I. The energies at 0p-0h are the values of  $E_{\text{sph}}$  and  $E_{\text{def}}$  shown in the same Table I. The  $E_{\text{def}}$  is much lower than  $E_{\text{sph}}$ , but  $\langle J^2 \rangle$  for the deformed SD is as large as 20.35, far away from  $\langle J^2 \rangle = 0$  of the spherical HF state. At the 2p-2h truncation level, the spherical CI energy drops very close to that of the deformed CI, while the latter is struggling for recovering the angular momentum, and  $\langle J^2 \rangle$  drops to 11.30. At the 4p-4h truncation level, the spherical CI energy is even lower than the deformed ones, yet the angular momentum of the latter hasn't been completely recovered. The advantage of the deformed mean field is then completely lost in the CI due to the lack of good angular momentum. At the 8p-8h truncation level the deformed CI state completely recovers its angular momentum, and the results from spherical CI and deformed CI become equivalent. Thus, we conclude that the deformed CI won't benefit from the deformed mean field unless the angular momentum is recovered from the outset. The PCI method described in Section II maintains the advantages of the deformed mean field and of configuration mixing specific to CI, and could provide further improvement to the  $E_{\text{pj}}(I=0)$  in Table I.

To describe those non-zero spin states, one can change the spin from 0 to  $I$  in Eq. (21), and keep  $s$  and  $\epsilon$  unchanged. Then one gets a sequence of energies,  $E_{\text{pj}}(I)$  shown as D=1 in Fig. 4. One can see that the values of  $E_{\text{pj}}(I)$  have approximately reproduced the  $I(I+1)$  feature of a rotational band in the low spin region. The 2 MeV gap between the D=1 band and the Full CI band is expected to be reduced by taking advantage of the CI techniques, in which the interaction between different intrinsic configurations has been properly considered. Results of the PCI for different bases are also shown in Fig. 4. First, we take 41 projected SDs having the same configuration ( $s_0$ ), but different shapes, as in the GCM method. The 41 shapes considered are taken from  $\epsilon_2 = -0.6$  to 0.6 by a step of 0.03, and  $\epsilon_4$  is obtained by minimizing the energy of Eq.(21) with  $I=0$  at each  $\epsilon_2$ . One can see that the calculated g.s. band is not

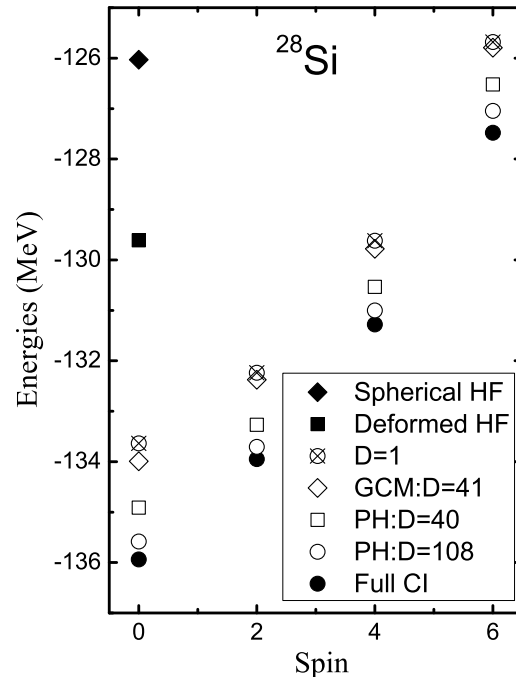


FIG. 4: Calculations of the ground state band in  $^{28}\text{Si}$  with different basis. Except for the GCM:D=41 case, the deformation for all the other cases is  $(\epsilon_2 = -0.40, \epsilon_4 = -0.20)$

improved. This can be understood by the large overlap between the PSDs in the GCM basis, therefore, the effective dimension of the basis is far below 41. Adding more PSDs with new shapes in the basis doesn't make much improvement. Therefore, we considered up to  $2p-2h$  excitations of the deformed  $s_0$  configuration used in the D=1 case, and built a PCI basis by selecting D=40 SDs (see next section). With this basis we solved the generalized eigenvalue problem described in Section II. The results (PH:D=40) in Fig. 4 indicate a significant improvement over GCM (GCM:D=41). As the number of excited PSDs increases up to 107, we obtain the band (labeled by PH:D=108), which is only about 300 keV above the band obtained with full CI. Therefore, we con-



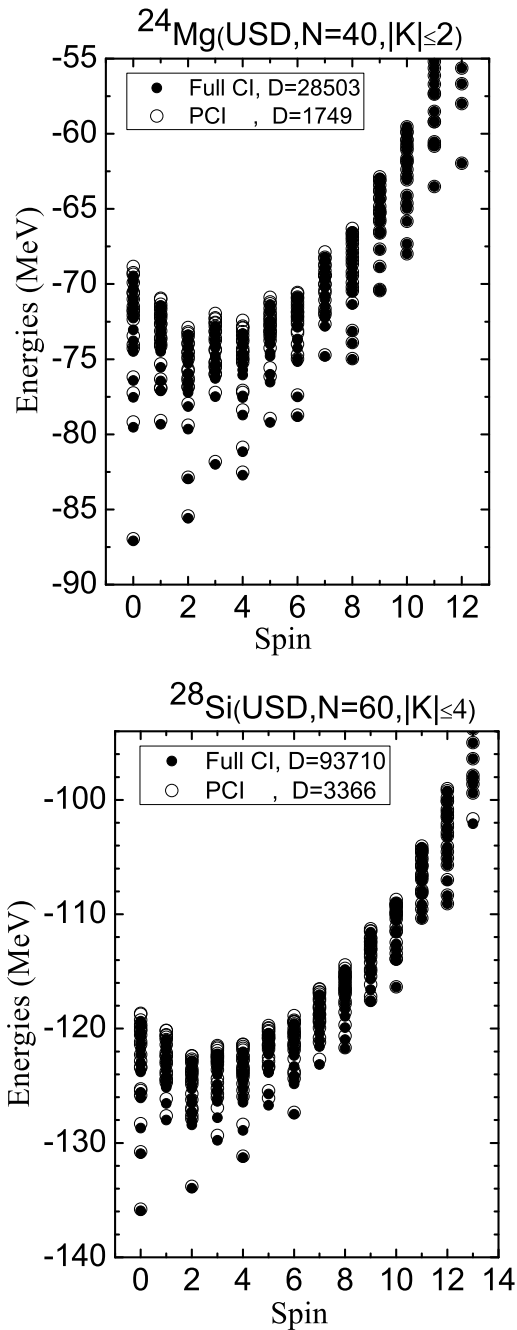


FIG. 7: Energies for  $^{24}\text{Mg}$  and  $^{28}\text{Si}$  calculated using PCI (open circles) and full CI (filled circles). 20 energies for each spin are presented.

In this way we constructed the basis for the PCI calculations of  $^{24}\text{Mg}$  and  $^{28}\text{Si}$  in the  $sd$  shell. For the  $^{24}\text{Mg}$ , we included  $N = 40$  lowest energy  $|\kappa_j, 0$  SDs with  $|K| \leq 2$ , and 1749 SDs are selected for the basis when  $E_{\text{cut}} = 10$  keV. For the  $^{28}\text{Si}$  case,  $N = 60$ ,  $|K| \leq 4$  and  $E_{\text{cut}} = 10$  keV selects 3366 SDs. The choice of  $|K| \leq 2$  seems to be arbitrary, and at this point it is related to the number of states one wants to include in the basis. One should

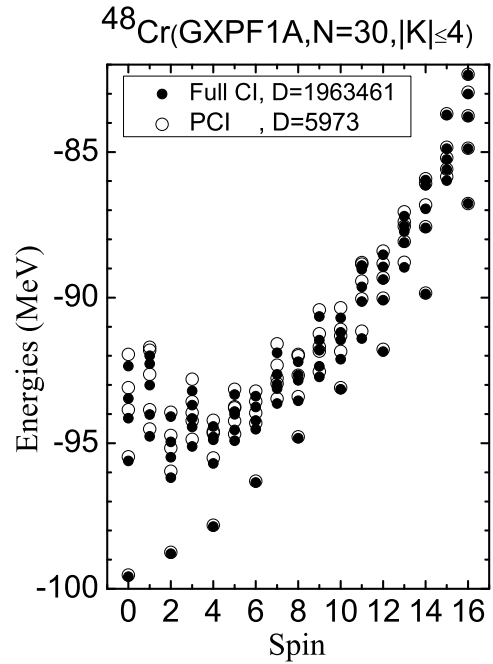


FIG. 8: The lowest 5 energies at each spin for  $^{48}\text{Cr}$  calculated using PCI (open circles) and full CI (filled circles).

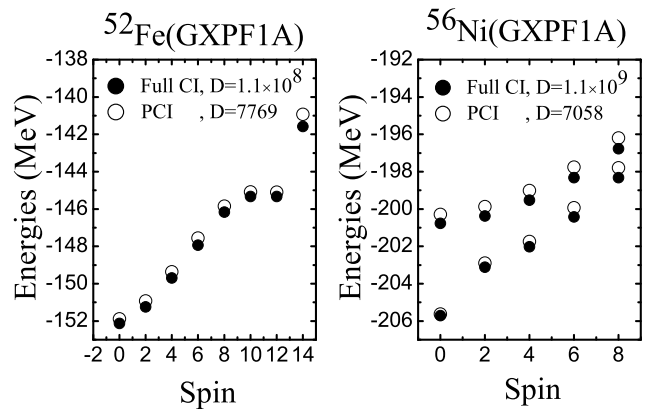


FIG. 9: Calculated yrast band energies using PCI (open circles) and full CI (filled circles) for  $^{52}\text{Fe}$  and  $^{56}\text{Ni}$ . The deformed band in  $^{56}\text{Ni}$  starting around 5 MeV is also shown (see text for details).

emphasize that the PCI method combines the advantage of using a set of s.p. bases of different deformations with that of the CI  $np-nh$  configuration mixing. In  $m$ -scheme CI, for example, one can get the states for all spins using the lowest  $M$  value (0 for even-even cases), although using higher  $M$  values could be somewhat more efficient for higher spins. In PCI one has to weigh in the advantages of using a larger number of  $np-nh$  excitations with those of using larger  $K$  values for larger spins. Using our choices for the  $K$  values the lowest 20 PCI energies of each spin are compared in Fig. 7 with the full CI results. Almost all low-lying energies for each spin reproduce the

full CI results very well. We conclude that the selected PCI basis has already carried almost the whole information of the low-lying states, yet we chose only a small number of SDs as compared with those used in the full  $m$ -scheme CI.

The QMCD [13] method also uses a relatively small number of selected SDs. For a basis of 800 SDs QMCD found a g.s. energy of  $-89.91$  MeV for  $^{24}\text{Mg}$ . In the present calculation, after the orthogonalization of the 524  $K = 0$  SDs, 453 SDs are used to calculate the  $I=0$  energies (see Table III). The resulting PCI g.s. energy is  $-89.94$  MeV. Furthermore, the QMCD paper only reports the 6 lowest states with spin up to  $I = 4$ , while our PCI calculation with the selected 1749 SDs can provide tens of excited states with spin running from 0 to 12 that compare well with the full CI results. Our approach seems to largely extended the range of nuclear states that can be calculated using a relatively small basis.

The results for  $^{28}\text{Si}$  are similar to those of  $^{24}\text{Mg}$ . Comparing with the  $N = 1$  calculation, that has been discussed in Section III, the dimension is much larger because one needs to describe a large number of low-lying states of the same spin. For  $I = 0$  the number of  $K = 0$   $|\kappa_j, 0\rangle$  SDs is  $N = 15$ , and a total of 747 independent SDs are selected from the 886  $K = 0$  SDs. The first 20  $0^+$  states, up to about 18 MeV excitation energy, are reasonably close to the full CI results. For  $I \neq 0$  the situation is very much the same.

The  $pf$  calculations show similar trends. For  $^{48}\text{Cr}$ , the CI  $m$ -scheme dimension is 1963461. Full CI calculations can reproduce the rotational nature of the yrast band and its backbending [20]. With PCI we choose  $N = 30$ ,  $|K| \leq 4$ , and for  $E_{\text{cut}} = 0.2$  keV 5973 SDs were selected. The lowest 5 energies for each spin are compared with the full CI results in Fig. 8. Again, we reached a satisfactory agreement between PCI and full CI.

$^{52}\text{Fe}$  and  $^{56}\text{Ni}$  are not good rotors, and the present choice of the basis is not so efficient as for  $^{48}\text{Cr}$ . However, one can still select a PCI basis that can provide a reasonable description of the yrast energies when compared with the full CI calculations, as shown in Fig.9. The number of deformed SDs used in these calculations is about 7000, which is just a small fraction of the full CI  $m$ -scheme dimension for  $^{52}\text{Fe}$ , and for  $^{56}\text{Ni}$  (see Table III). However, the choice of the PCI basis for  $^{52}\text{Fe}$  and  $^{56}\text{Ni}$  needs to be improved. Details will be presented in the forthcoming paper.

For  $^{56}\text{Ni}$  a rotational band has been identified in experiment [21] that starts at around 5 MeV excitation energy. The band was successfully described by full CI calculations in the  $pf$ -shell using the GXPF1A interaction[17]. It was also shown [17] that this band has a 4p-4h character, but in order to get a good description of the band 10p-10h excitations from  $(f_{7/2})^{16}$  configuration are necessary. In the present PCI calculation this rotational band has been identified (see Fig. 9) in the calculated excited states by inspecting the quadrupole moments and the  $B(E2)$  transitions (See Table II). The results seem to

TABLE II: Quadrupole moments (in  $efm^2$ ) and  $B(E2, I \rightarrow I - 2)$  (in  $e^2fm^4$ ) values of the states in the deformed band of  $^{56}\text{Ni}$  calculated with PCI and CI. The energies for  $I \neq 0$  are relative to the  $I = 0$  bandhead. The CI values are taken from Ref. [17]

Spin	Energy (MeV)		$Q(I)$		$B(E2)$	
	PCI	CI	PCI	CI	PCI	CI
0	-200.295	-200.762	0	0		
2	0.425	0.395	-48.9	-41.6	567.1	413.2
4	1.312	1.241	-44.0	-55.2	646.0	598.0
6	2.541	2.448	-70.5	-56.2	708.0	609.3
8	4.103	3.991	-74.5	-47.2	938.6	558.4

TABLE III: PCI Dimensions for several spins compared with those of full CI for the nuclei described in this Section.

Nucleus		$I = 0$	$I = 2$	$I = 4$	$I = 6$
$^{24}\text{Mg}$	SM	1161	4518	4734	2799
	PCI	453	1569	1579	1492
$^{28}\text{Si}$	SM	3372	13562	15089	9900
	PCI	747	2266	2919	2711
$^{48}\text{Cr}$	SM	41355	182421	246979	226259
	PCI	1671	3888	5618	5594
$^{52}\text{Fe}$	SM	$1.8 \times 10^6$	$8.0 \times 10^6$	$1.2 \times 10^7$	$1.2 \times 10^7$
	PCI	4288	6422	6811	6806
$^{56}\text{Ni}$	SM	$1.5 \times 10^7$	$7.1 \times 10^7$	$1.1 \times 10^8$	$1.1 \times 10^8$
	PCI	2373	3968	5452	6231

be in reasonable good agreement with those of the full CI calculations. The details about the calculation of the quadrupole moments and the  $B(E2)$  transitions are given in the next section.

The number of SDs selected for the PCI calculation are shown in the corresponding figures and compared with the full CI  $m$ -scheme dimensions. However, the efficiency of the PCI truncation can also be assessed by comparing the PCI dimensions with the coupled-I CI dimensions. In PCI the states used for the diagonalization of each spin in Eq. (12) are obtained from the selected PSDs after the latter are orthogonalized and the redundant states are filtered out. The remaining states form the PCI basis for each spin. These dimensions are compared in Table III with the full coupled-I CI dimensions. One can see that PCI can provide reasonable good results using much smaller dimensions than the corresponding  $m$ -scheme and/or coupled-I CI calculations.

Although the PCI calculations could have much smaller dimensions than those of the corresponding full CI calculations, the  $H$  and  $N$  matrix in Eq. (12) are dense. To get an idea of the workload of a PCI calculation, the time necessary to calculate the  $H$  and  $N$  matrices for  $^{56}\text{Ni}$  at  $I=0, 2, 4, 6, 8$  takes around 8 hours using one processor, and the calculation of 5 eigenvalues for each spin takes about 2 hour, when the generalized Lanczos method is used. As a comparison, the full CI calculations of the same states using the modern coupled-I code NuShellX [22] could take several weeks, when one



processor is used. One should also observe that the PCI computational load is shifted towards the calculation of the matrix elements, which can be more efficiently parallelized than any large matrix eigenvalue solver.

## V. QUADRUPOLE MOMENTS AND BE2 TRANSITIONS

The quadrupole moments and  $B(E2)$  transitions are given by

$$\begin{aligned} Q(I) &= \sqrt{\frac{16\pi}{5}} \langle \Psi_{IM=I} | \hat{Q}_{20} | \Psi_{IM=I} \rangle \\ &= \sqrt{\frac{16\pi}{5}} \langle II, 20 | II \rangle \langle \Psi_I | | \hat{Q}_2 | | \Psi_I \rangle \end{aligned} \quad (24)$$

$$\begin{aligned} B(E2; I_i \rightarrow I_f) &= \frac{2I_f + 1}{2I_i + 1} |\langle \Psi_{I_f} | | \hat{Q}_2 | | \Psi_{I_i} \rangle|^2 \\ &= |\langle \Psi_{I_i} | | \hat{Q}_2 | | \Psi_{I_f} \rangle|^2 \end{aligned} \quad (25)$$

where

$$\hat{Q}_{\lambda\mu} = e_{n(p)} r^2 Y_{\lambda\mu}(\theta, \phi), \quad (26)$$

with effective charges taken as  $e_n = 0.5e$ ,  $e_p = 1.5e$ . The reduced matrix element in Eq.(24) and (25) can be expressed in terms of the PCI wave functions

$$\begin{aligned} &\langle \Psi_{I_f} | | \hat{Q}_2 | | \Psi_{I_i} \rangle \\ &= \sum_{K\kappa, K'\kappa'} f_{I_i K\kappa} f_{I_f K'\kappa'} R_{I_f K'\kappa', I_i K\kappa}, \end{aligned} \quad (27)$$

where

$$R_{I_f K'\kappa', I_i K\kappa} = \sum_{\nu} \langle I_i K' - \nu, \lambda\nu | I_f K' \rangle \langle \Phi_{\kappa'} | \hat{Q}_{\lambda\nu} P_{K' - \nu, K}^{I_i} | \Phi_{\kappa} \rangle \quad (28)$$

Explicit expression for the  $\langle \Phi_{\kappa'} | \hat{Q}_{\lambda\nu} P_{K' - \nu, K}^{I_i} | \Phi_{\kappa} \rangle$  can be found in Ref. [7]. Here  $\langle I_i K' - \nu, \lambda\nu | I_f K' \rangle$  is a Clebsh-Gordon coefficient.

Using the PCI wave functions for the states shown in Fig.7 and Fig.8, we calculated the  $Q(I)$  and the  $B(E2)$  values for the yrast band in  $^{24}\text{Mg}$ ,  $^{28}\text{Si}$  and  $^{48}\text{Cr}$ . The results are shown in Fig.10. The very good agreement between PCI and full CI indicates that the PCI wave functions are almost equivalent to the exact ones.

## VI. CONCLUSIONS AND OUTLOOK

In this paper we investigate the adequacy of using a deformed s.p. basis for CI calculations. We show that even if the starting energy of the deformed mean-field is lower than the spherical one, the series of  $np - nh$  truncations in the deformed basis exhibits slower convergence than

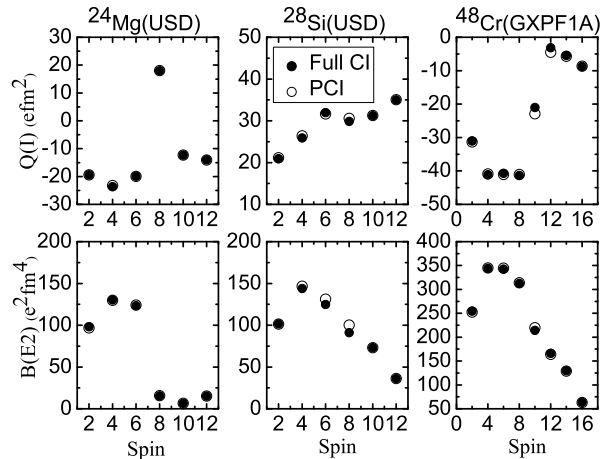


FIG. 10: Calculated quadrupole moments (upper panel) and  $B(E2)$  (lower panel) from PCI (open circles) and full CI (filled circles) for  $^{24}\text{Mg}$ ,  $^{28}\text{Si}$  and  $^{48}\text{Cr}$ .

that of the spherical basis, due to the loss of rotational invariance that is not recovering fast enough.

Therefore, we propose a new strategy called Projected Configuration Interaction (PCI) that marries features of GCM, by projecting on good angular momentum SDs built with deformed s.p. orbitals, with CI techniques, by mixing a large number of appropriate deformed configurations and their  $np - nh$  excitations. This ansatz seems to be very successful in describing not only the yrast band, but also a large class of low-lying non-yrast states. This method seems to work extremely well for deformed nuclei, and it needs further improvements to the choice of the PCI basis for spherical nuclei.

For the  $sd$  and  $pf$ -shell nuclei that we studied we show that the quadrupole moments and the  $BE(2)$  transition probabilities are very well reproduced, indicating that not only the energies, but also the wave functions are accurately described. This suggests that this method could be helpful in finding relations between the intrinsic states, which offer more physics insight, and the laboratory wave functions provided by CI.

One of the simplifications that makes these calculations with tens of thousands of projected states possible is the approximation of the deformed mean-field with an axially symmetric rotor defined by its quadrupole and hexadecupole deformations. This approach seems to describe very well the HF mean field for the  $sd$  and  $pf$ -shell nuclei. We plan to extend our method to include octupole deformation, and to consider triaxial shapes.

## Acknowledgments

The authors acknowledge support from the DOE Grant No. DE-FC02-07ER41457. M.H. acknowledges support

from NSF Grant No. PHY-0758099. Z.G. acknowledges the NSF of China Contract Nos. 10775182, 10435010 and 10475115.

- 
- [1] B. H. Wildenthal, *Prog. Part. Nucl. Phys.* **11**, 5 (1984).  
 [2] B.A. Brown and B.H. Wildenthal, *Ann. Rev. Nucl. Part. Sci.* **38**, 29 (1988).  
 [3] A. Poves, and A. P. Zuker, 1981a, *Phys. Rep.* **71**, 141.  
 [4] W. A. Richter, M. J. van der Merwe, R. E. Julies, and B. A. Brown, 1991, *Nucl. Phys. A* **523**, 325.  
 [5] M. Honma, T. Otsuka, B. A. Brown, and T. Mizusaki, *Phys. Rev. C* **65**, 061301(R)(2002).  
 [6] J. P. Elliott, *Proc. R. Soc. London, Ser. A* **245**, 128,562(1958).  
 [7] K. Hara and Y. Sun, *Int. J. Mod. Phys. E* **4**,637(1995).  
 [8] S. G. Nilsson. *Dan. Mat. Fys. Medd* **29** nr.16(1955)  
 [9] Y. S. Chen and Z. C. Gao, *Phys. Rev. C* **63** 014314(2000).  
 [10] J.A. Sheikh and K. Hara, *Phys. Rev. Lett.* **82**, 3968(1999).  
 [11] Z. C. Gao, Y. S. Chen, and Y. Sun, *Phys. Lett.* **B634** 195(2006)  
 [12] K.W. Schmid, *Prog. Part. Nucl. Phys.* **52**, 565(2004)  
 [13] M. Honma, T. Mizusaki, and T. Otsuka, *Phys. Rev. Lett.* **77**, 3315 (1996).  
 [14] S. E. Koonin, D. J. Dean, and K. Langanke, *Phys. Rep.* **278**, 2(1997).  
 [15] D. L. Hill and J. A. Wheeler, 1953, *Phys. Rev.* 89, 1102.  
 [16] M. Hjorth-Jensen, T. T. S. Kuo and E. Osnes, *Phys. Rep.* **261**, 125 (1995).  
 [17] M. Horoi, B. A. Brown, T. Otsuka, M. Honma, and T. Mizusaki, *Phys. Rev. C* **73** 061305(R)(2006).  
 [18] Y. Alhassid, G. F. Bertsch, L. Fang and B. Sabbey, *Phys. Rev. C* **74** 034301(2006)  
 [19] R. Rodriguez-Guzmán, Y. Alhassid and G.F. Bertsch, *Phys. Rev.* **77**, 064308 (2008).  
 [20] E. Caurier et al., *Phys. Rev. Lett.* 75, 2466 (1995).  
 [21] D. Rudolph et al., *Phys. Rev. Lett.* 82, 3763 (1999).  
 [22] W.D.M. Rae, NuShellX code 2008, <http://knollhouse.org/NuShellX.aspx>